# Payload hardware and experimental protocol for testing the effect of space microgravity on the resistance to gentamicin of stationary-phase uropathogenic *Escherichia coli* and its $\sigma^s$-deficient mutant

AC Matin*, J-H Wang, Mimi Keyhan, Rachna Singh, Michael Benoit

Department of Microbiology & Immunology, Stanford School of Medicine,

Stanford, CA 94305, USA

Macarena P. Parra,* Michael R. Padgen, Antonio J. Ricco,* Matthew Chin,
Charlie R. Friedericks, Tori N. Chinn, Aaron Cohen, Michael B. Henschke,
Timothy V. Snyder, Matthew P. Lera, Shannon S. Ross, Christina M. Mayberry,
Sungshin Choi, Diana T. Wu, Ming X. Tan, Travis D. Boone, Christopher C.
Beasley, and Stevan M. Spremo

NASA Ames Research Center, Moffett Field, CA 94035, USA

*Corresponding author: a.matin@stanford.edu

*Other corresponding authors: macarena.p.parra@nasa.gov ,
antonio.j.ricco@nasa.gov

# ABSTRACT

Human immune response is compromised and bacteria can become more antibiotic resistant in space microgravity (MG). We report that under low-shear modeled microgravity (LSMMG) stationary-phase uropathogenic *Escherichia coli* (UPEC) become more resistant to gentamicin (Gm). UPEC causes urinary tract infections (UTIs), reported to afflict astronauts; Gm is a standard treatment, so these findings could impact astronaut health. Because LSMMG has been shown to differ from MG, we report here preparations to examine UPEC's Gm sensitivity during spaceflight using the *E. coli Anti-Microbial Satellite* (*EcAMSat*) on a free-flying "nanosatellite" in low Earth orbit. Within *EcAMSat's* payload, a 48-microwell fluidic card contains and supports study of bacterial cultures at constant temperature; optical absorbance changes in cell suspensions are made at three wavelengths for each microwell and a fluid-delivery system provides growth medium and predefined Gm concentrations. Performance characterization is reported for spaceflight prototypes of this payload system. Using conventional microtiter plates, we show that Alamar Blue (AB) absorbance changes due to cellular metabolism accurately reflect *E. coli* viability changes: measuring AB absorbance onboard *EcAMSat* will enable telemetry of spaceflight data to Earth. Laboratory results using payload prototypes are consistent with wellplate and flask findings of differential sensitivity of UPEC and its Δ*rpoS* strain to Gm. Space MG studies using *EcAMSat* should clarify inconsistencies from previous space experiments on bacterial antibiotic sensitivity. Further, if $\sigma^s$ plays the same role in space MG as in LSMMG and Earth gravity, *EcAMSat* results would facilitate utilizing our previously-developed terrestrial UTI countermeasures in astronauts.

## KEYWORDS

Bacterial antibiotic resistance; microgravity; low-shear modeled microgravity (LSMMG); stress response; sigma S; stationary phase; uropathogenic *E. coli* (UPEC); *EcAMSat*; nanosatellite; cubesat; gentamicin; alamar blue; sigma-s deletion.

## INTRODUCTION

When *Escherichia coli* experiences stationary phase under Earth gravity, it induces the general stress response (GSR), which makes it comprehensively resistant against a variety of disinfectants.[1-4] GSR is controlled by the master regulator of this response, sigma S ($\sigma^s$, encoded by the *rpoS* gene). This sigma factor controls the synthesis of a core set of proteins that protect vital cell biomolecules, i.e., proteins, DNA, and the cell envelope.[3,4]

Like disinfectants, antibiotics cause cytotoxicity by damaging the biomolecules that the $\sigma^s$-controlled proteins protect. We therefore recently tested the effect of the loss of this sigma factor on the sensitivity of stationary-phase uropathogenic *E. coli* (UPEC) to the antibiotic, gentamicin (Gm): the $\sigma^s$-deficient strain did indeed show enhanced sensitivity to the drug relative to the unmodified strain.[5]

*E. coli* cultivated under what is often referred to as low-shear modeled microgravity (LSMMG), generated by the use of high-aspect-ratio vessels (HARVs), also develop a $\sigma^s$-dependent comprehensive resistance, which resembles GSR.[6] We note that the conditions in

HARVs are more precisely described as 'low-shear cell suspension', a term indicative of the absence of gravitational cell sedimentation due to the flow of medium past the cells at low interfacial shear rates. We will, however, continue to use the term LSMMG, which has been widely adopted to describe such experiments. LSMMG-grown *E. coli* become more resistant to high salt, low pH, and ethanol[5-7] and, as we show here for UPEC, also to Gm.

UPEC is a causative agent of urinary tract infection (UTI), for which Gm is standard treatment. UTI has been reported in astronauts.[8] Therefore, if the LSMMG findings are applicable to actual microgravity of space (MG), they would indicate a potential threat to space travelers, especially since there is growing evidence that the human immune response is weakened by MG.[9-11] However, LSMMG may not have full fidelity to space MG, and it is thus necessary to examine Gm sensitivity of UPEC in *in-situ* space experiments.

Biological experiments on the Space Shuttle and the International Space Station (ISS) can be limited and costly because of crewmember involvement and other factors. NASA has therefore developed fully autonomous microsystems in the form of free flying "nanosatellites" for space experimentation. Examples are: *GeneSat*, *PharmaSat*, and *O/OREOS*.[12-15] These platforms avoid astronaut involvement and permit experimentation in more orbital locations than ISS. *PharmaSat* has been used to measure the effects of low-Earth-orbit microgravity ($< 10^{-3}$ x Earth gravity) on the sensitivity of the yeast *Saccharomyces cerevisiae* to the antifungal agent voriconazole.[13,14] We have modified *PharmaSat* for experiments with bacteria in order to determine *E. coli* sensitivity in space to Gm. The modified payload system (referred to as *EcAMSat*, short for *E. coli* Antimicrobial Satellite) and tests of its suitability for space experiments are described here.

Given the findings of Wang et al.[5] under Earth gravity of the involvement of $\sigma^s$ in Gm resistance, we have included in these studies the Δ*rpoS* mutant of UPEC, missing $\sigma^s$. Should it turn out that the enhanced resistance of UPEC to Gm in MG also depends on this sigma factor, it would indicate new ways of controlling UPEC resistance to Gm during space flight.

We have focused on stationary-phase bacteria in this and our previous studies[4,5,16] for the following reasons: a) bacteria in this phase are hard to eradicate; b) due, for example, to lack of nutrient or the presence of oxidative stress, this late-growth phase is often experienced by bacteria in the human host;[1-3,17] and c) stationary-phase bacteria express virulence traits required for disease causation;[18-24] an example is UPEC Type I fimbriae, which it uses in bladder colonization.[25, 26]

## MATERIALS AND METHODS

**LSMMG effect on Gm sensitivity.** To determine the effects of cultivation under LSMMG on Gm sensitivity, the wild type and the Δ*rpoS* UPEC strains were cultivated in HARV reactors as described previously.[6] Pairs of the reactors were rotated about appropriate axes: vertical for normal gravity ('HARV NG') and horizontal for LSMMG conditions. 50 mL of Luria broth (LB) medium was used in each vessel. Overnight conventional-flask LB cultures were used as inoculum; the starting absorbance at 660 nm ($A_{660}$) was 0.1, and the HARVs were rotated at 25 revolutions per minute. Following 24-h incubation (37 °C), the stationary-phase cells were harvested from the HARVs, re-suspended in M9 salts (referred to from hereon as 'M9') to an $A_{660}$ of 0.4, and mixed with sufficient Gm to give a final concentration of 16 µg/mL. After 24-h incubation (37 °C) under static conditions, viability was determined by counting colony-forming units (CFU) using LB plates.

**Determination of the suitability of Alamar Blue to assess Gm effect on UPEC viability.** To test the effect of space MG in inflight experiments, a method for UPEC viability assessment is needed, the results of which can be transmitted from space to Earth via telemetry. The dye Alamar Blue (AB) was used as a reporter for this purpose in the *PharmaSat* mission concerning yeast viability mentioned above.[14] The yeast cell metabolic activity resulted in AB reduction, causing its color to change from dark blue to magenta, thus increasing absorption at 525 and decreasing it at 615 nm; from this conversion the relative change in cell viability could be assessed.[12] Concomitant measurement at 470 nm, where absorbance is weak for both reduced and oxidized forms of AB, indicated solution turbidity and thus cell population.

Measured absorbance at 615, 525, and 470 nm only approximates the respective amounts of oxidized AB, reduced AB, and cell-related turbidity. To more accurately determine these parameters, we measured complete visible absorbance spectra of oxidized AB, reduced AB, and a suspension of *E. coli*. We then used the absorbance values at the three measurement wavelengths to calculate "cross terms" that correct for the fact that the absorbance spectrum of (blue) oxidized AB has a shoulder at 525 nm and a tail at 470 nm, that the spectrum of (magenta) reduced AB also has a tail at 470 nm, and that light scattering by the bacteria occurs throughout the visible range, varying with a weak linear wavelength dependence. All graphics and results reported below for quantities of oxidized AB, reduced AB, and cell turbidity have been corrected accordingly.

To determine if the AB-conversion method can be used for assessing UPEC viability, the wild type and its isogenic Δ*rpoS* mutant[5] were grown in conventional laboratory flasks shaken overnight at 200 rpm in 1/6-strength LB at 37 °C. As before,[16] growth under these conditions was complete within 6 hours, allowing some 8 hours of starvation in stationary phase; this starvation period permits activation of GSR in the wild type.[27] The cultures were then diluted to an $A_{600}$ of 0.45 in M9. Gm (Sigma-Aldrich, St. Louis, MO) was added to both the wild type and the mutant cultures to a final concentration of 16 µg/mL; a parallel aliquot of cell suspension of each strain without the drug served as control. Following 24-h incubation without shaking, 1.8 mL of the cultures were transferred to test tubes to which 200 µL of 10x AB (ThermoFisher Scientific, Grand Island, NY) was added. To monitor changes in AB absorption, the cultures were dispensed in microtiter plate wells (Figure 3B; Thermo Scientific, Waltham, MA), each well receiving 0.25 mL. Appropriate control solutions in other rows of the well plates were also in 0.25 mL quantities, and five wells were used for each condition. Absorption changes at 470, 525, and 615 nm were measured in a microplate reader (Biochrom US, Holliston, MA); data were acquired by DigiRead software (ASYS Hitech, Holliston, MA) and transferred to Excel (Microsoft, Redmond, WA) for analysis.

***EcAMSat* payload system.** In this system, the *E. coli* cells are placed in the payload hardware in a 48-well fluidic card (Figure 1; Micronics, Redmond, WA). The cards are made from laser-cut layers of poly(methylmethacrylate) bonded together with pressure-sensitive acrylic adhesive (9471LE on 51-µm-thick Melinex 455 polyester carrier, 3M; St. Paul, MN). Each well (4.0 mm diameter x 7.8 mm long; 100 µL volume) is fitted at its inlet and outlet with 0.2-µm filters (nylon fiber; Sterlitech, Kent, WA) to prevent cell leakage. Well tops and bottoms are sealed by 50-µm-thick air-and-$CO_2$-permeable optical-quality poly(styrene) membranes. Attached to both sides of the card are thermal spreaders (thin aluminum plates), each containing three embedded AD590 temperature sensors that provide output current directly proportional to absolute temperature (Analog Devices, Norwood, MA); a thin-film heater fabricated from kapton tape and patterned metal conductors (Minco, Minneapolis, MN) is affixed to the opposite side of each spreader plate, relative to the fluidic card, and controlled in a closed-loop fashion using the temperature sensor outputs. Each well is equipped with its own 3-color LED (LTST-

C17FB1WT; Lite-On Technology Corp., Taiwan); a photodetector (Model no. TSL237T; AMS-TAOS USA, Plano, TX) at the opposite end of each well converts the transmitted light intensity to a proportional frequency, from which absorbance values can be calculated. (No moving parts are associated with the optical measurements.) The card, thermal spreaders, and printed-circuit (PC) boards supporting the LEDs and photodetectors, which are placed on opposite sides of the fluidic card, constitute the "card stack" (see the cross section, upper right in Figure 1).

The card fluid-delivery system (Figure 1) includes 11 electrically-actuated solenoid valves (SVs, LHDA0531315HA; The Lee Co., Westbrook, CT); a diaphragm pump for high-flow-rate fluid mixing, circulation, and priming of tubing (NF 5S; KNF Neuberger, Trenton, NJ); a precision metering pump (LPVX0502600BC; The Lee Co.) to prepare and deliver the desired concentrations and volumes of antibiotic and other reagents; three 35-mL and six 25-mL reagent bags (fluorinated ethylene propylene, FEP; American Fluoroseal/Saint-Gobain, Gaithersburg, MD); a bubble trap (custom fabricated by NASA Ames); and a check valve (Smart Products; Morgan Hill, CA) to prevent waste fluids from flowing back into the system. The 48 wells are configured in 4 fluidically independent rows or "banks" of 12 each (labeled "High", "Medium", "Low", and "Control" in Figure 1, indicating the relative Gm concentrations that were administered). Each bank on the inlet side of the card is connected to the normally-closed port of one SV and, on the outlet side, to a 25-mL waste bag partially filled with M9 salts (without glucose; Sigma-Aldrich, St. Louis, MO; referred to from hereon as 'M9'); pressurization (~7 kPa) of these waste bags by means of a spring-loaded metal plate replaces any fluid that evaporates over time from the wells through their permeable membrane cover. The nutrient (1/6-strength LB), antibiotic (Gm), antibiotic dilution medium (M9), and AB bags are also attached to SV NC ports (Figure 1). A Gm-dilution loop is created by attaching the M9 bag via another SV near the outlet of the bubble trap, which is placed ahead of the point of fluid delivery to the card. The main waste bag collects the previous contents of the tubing each time it is filled with a new reagent (see below) prior to delivery to the card.

Figures 2A and 2B show, respectively, the assembled *EcAMSat* payload fluidic system hardware and the hermetically sealed containment vessel (internal volume ~ 1.2 L) in which the system is housed. The sealed payload containment vessel is integrated with the spacecraft "bus", which includes the power, communications, data-handling, and control functions. The completed nanosatellite has overall dimensions of 10 x 22 x 36 cm.

**AB-mediated assessment of Gm effect in the *EcAMSat* payload on Earth.** The wild type and Δ*rpoS* mutant of UPEC were grown as described above, rinsed with M9 (3x), and diluted in M9 to an $A_{600}$ of 1.0. In a sterile biosafety cabinet, 5 µL aliquots of each strain were loaded in alternating wells of the 48-well fluidic card so that six of the 12 wells per bank contained the wild type and six the mutant. The card was sealed and purged with $CO_2$ to facilitate bubble-free filling of the channels and wells: any $CO_2$ bubbles remaining after priming with degassed M9 dissolved readily as additional M9 flowed through the wells. The card was manually primed with a syringe containing degassed M9 connected to the outlet, and a second empty syringe at the inlet, its plunger drawn back to generate a slight vacuum. After filling and until connection to the fluidic system, the card remained under pressure (~4.4 kPa) from a bag of M9 hanging approximately 45 cm above the card; this served to replace any fluid lost by evaporation through the permeable membranes and thereby prevented bubble formation in the wells. The rest of the sterile fluidic system was filled with the appropriate solutions (see Figure 1), assembled with the rest of the payload hardware, and then sealed in the hermetic containment vessel; as explained above, slightly pressurized M9 in the waste bags continued to compensate for any evaporation. As placement in the containment vessel eliminated further need for a sterile environment, the assembled payload system was removed from the biosafety cabinet and attached to a benchtop “rotisserie” apparatus; this rotated the payload first clockwise and then counterclockwise by nearly one full rotation with a period of ~ 80 s, preventing cell settling. The experiments were run using ground-support equipment, i.e., a desktop computer and power supply, and employed a “space-flight-like” command sequence.

To start the viability measurements, the 3-color LEDs with emissions at the above-mentioned wavelengths were sequentially energized, one color and one well at a time. The photodetector of each well converted the transmitted light intensity of each color to a proportional frequency, permitting calculation of absorbance. (During the spaceflight experiments, the stored frequencies will be telemetrically transferred to Earth from the satellite.) The measurements for each well were taken every 15 min. The payload system was warmed to 37 °C for ~3 hours (Figure 2C) by the heaters and thermal spreaders with closed-loop temperature control using the mean value from the six temperature sensors. 1/6-strength LB was pumped into each bank in turn, starting with the control bank, replacing the M9. The pumping phase lasted for two hours per bank (see Results section for total durations of the various phases). The cells were allowed to grow to stationary phase and then to starve. Next, the metering pump delivered M9 to the control bank; each well received ~ 4x its 100 µL volume to reach at least 90% exchange. The metering pump then extracted a small, measured amount of concentrated Gm from the antibiotic bag and delivered it to the M9 dilution bag (Figure 1); the Gm-dilution loop was opened and the diaphragm pump operated to mix the antibiotic and M9. After delivery of the resultant lowest concentration of Gm to the Low bank (~4x exchange), the process was repeated to deliver the medium and high Gm concentrations to the Medium and

High banks, respectively. Following incubation with Gm, AB was added, displacing the M9 in the Control bank and the Gm in the other banks.

**Determination of 'stasis' effect.** An approximately six-week delay is expected between loading of cells and reagents into the satellite hardware and initiation of the experiments in space. To determine the effect of such stasis on cell viability, Gm strength, and AB properties, the cells were incubated without shaking in M9 for 10 weeks and the reagents were stored for this duration in the same types of bags that will be used for the space mission. Cell viability was determined by cell count; the Gm and AB activities were assessed by comparing the effect of aged reagents with fresh ones in cell killing and assessing cell activity, respectively.

## RESULTS

**LSMMG cultivation makes UPEC more resistant to Gm but not its Δ*rpoS* mutant.** We examined the effect of LSMMG cultivation on Gm sensitivity of UPEC: cells were cultivated in HARV reactors to stationary phase and then exposed to Gm for 24 h. LSMMG-grown UPEC was significantly more resistant to Gm than the control culture grown under HARV NG conditions (29 ± 2% vs. 18.6 ± 1.2% survival, $p < 0.01$). This is reminiscent of the well-established effect of LSMMG on enhanced resistance of *E. coli* to disinfectant agents.[6,8] Consistent with results with cells grown under NG in conventional flasks,[5] the Δ*rpoS* mutant was more sensitive to the drug than the wild type also under the HARV NG conditions (2.33 ± 0.09% vs. 18.6 ± 1.2% survival, $p < 0.01$). Furthermore, as in the case of disinfectant agents, the mutant, unlike the wild type, failed to show increased Gm resistance under LSMMG; indeed, under these conditions, it was more sensitive than its HARV NG-grown counterpart (0.21 ± 0.07% vs 2.33 ± 0.09% survival, $p < 0.001$).

Thus, LSMMG stress makes *E. coli* comprehensively resistant, including to an important drug, and this effect is $\sigma^s$-dependent. LSMMG may not fully represent space MG conditions, but given its relevance to these conditions, this finding constitutes a potential threat to astronaut health. This warrants corroboration under actual space MG to determine if countermeasures must be devised to safeguard astronaut health. Towards this end, the following experiments were carried out using the *EcAMSat* payload platform described in Materials and Methods.

**Alamar Blue absorption changes permit determination of UPEC viability.** As stated above (Materials and Methods), we tested AB as reporter for assessing cell viability to transmit results of the planned space experiments to Earth. For these experiments, our previous experimental protocol was used.[5] This entailed the following phases: growth, followed by starvation (needed to activate GSR), Gm treatment, and viability determination by CFU counts; in the present case, we substituted AB absorbance changes for the colony counting. The growth and starvation phases lasted 12 hours each, Gm treatment, 24 hours, and AB assessment of viability, 6 hours.

The results of the CFU counts of our previous work are reproduced in Figure 3A for convenience of reference;[5] they show that, compared to the wild type, Gm treatment causes a greater loss of viability in the UPEC strain missing the *rpoS* gene. Figure 3B shows the color changes of Alamar Blue in 96-well plates due to the metabolism of the treated and untreated wild type and Δ*rpoS* mutant strains (the rows of wells are aligned to the bars of Figure 3A representing the colony counts): it is clear that the AB absorption changes correlate well with the CFU counts.

Using a conventional well-plate reader, absorbance at 470, 525, and 615 nm was measured and used as described above to calculate the relative concentrations of the oxidized and reduced forms of AB and the optical density (turbidity) at the indicated time points. Figures 3C-F show these results when AB was used to assess the effect of Gm on the viability of the two strains; the controls (M9 alone and M9 + AB; data not shown in the figure) showed no change in absorbance. As indicated by lack of change in cell turbidity (black and grey curves; Figures 3C, D), no growth occurred during these experiments under any of the conditions. Pairwise comparisons, for the two strains, of the loss of blue AB or appearance of magenta AB with and without Gm (Figures 3C and 3D, respectively) yield $p < 0.0001$ in all four cases.

The concentrations of the blue (oxidized) form of AB for each strain and each condition are plotted vs. time in Figure 3E, which shows clearly that the amount of AB reduced by both strains when treated with Gm is less than for the respective untreated controls. Figure 3F compares the relative magnitude of the effect of the antibiotic on the wild type and mutant using the $t = 6$ hour results from Figure 3E. The heights of the bars are the percentages of AB reduced in the presence of Gm divided by the amount of AB reduced in the absence of Gm, for each strain. The results show that the Gm-treated wild type, which reduced 74.4 ± 2.2% of the amount of AB reduced by untreated wild type, differs significantly from Gm-treated mutant, which reduced 60.5 ± 3.2% of the amount of AB reduced by untreated mutant ($p < 0.001$). Thus, in both strains changes in AB absorption resulting from metabolic activity agree qualitatively with the Gm effect found by CFU measurements.

**The *EcAMSat* system permits efficient dilution and exchange.** It is of course essential that the dilutions and exchanges needed to conduct the experiments in the *EcAMSat* hardware be accurately accomplished. Antibiotic is carried in the payload in a concentrated form (400 µg/mL) and will require dilution to the planned three specific concentrations at the time of the space experiment. To determine antibiotic dilution accuracy, a 1% solution of non-toxic yellow dye (absorbance maximum ~ 414 nm) in M9 was loaded into the antibiotic bag in place of Gm (see Figure 2). The payload was assembled but not loaded into the hermetic containment vessel so that the system was in near-flight-like configuration but with the tubing accessible during pumping. Samples were obtained during pumping of the dye. The absorbance of each sample, diluted using the *EcAMSat* payload system, was measured at 414 nm, and the equivalent Gm dose was calculated using a standard curve. The accuracy of this dilution process was measured for three different "builds" of the fluidic system (i.e., different fluidic cards, sets of tubing, pumps, valves, etc.). Figure 4A shows measured dilutions using dye that correspond to Gm doses of 3.5, 14.6, and 52 µg/mL, corresponding to a systematic error of 9 – 16% below the intended concentrations; the coefficients of variance are 4 – 5% for the medium at high concentrations and 20% for the low; the latter is not unexpected due to its high dilution ratio. Because of the reasonably low degree of the deviations from the specified concentrations, and the fact that they will occur in both the spaceflight and ground control systems, they are not expected to significantly impact the results.

Fluid exchange in the banks is required to make transitions from initial stasis buffer to the following phases: feeding-and-starvation; Gm dosing; and finally AB-mediated viability measurement. To quantify the extent and consistency of these exchanges, 0.2% blue food dye in M9 was loaded in the AB bag and pumped into all four banks of the card using the same flow rate and duration as for the planned exchanges in the actual experiments (~4x volume exchange). The payload was then disassembled, and the absorbance of the dye at 620 nm was measured in the wells, using a well-plate reader. To ascertain the extent to which the replacement of M9 by the dye was less than 100%, the dye was introduced into the banks under pressure (4.4 kPa) to saturate the wells with it. The dye-filled bag was hung ~45 cm above the card and 6 mL of the dye was allowed to flow through each bank (~1.5 mL volume): subsequent measurement provided absorbance of the wells at 100% exchange. Background absorbance was determined following flushing the card with M9 (which has zero absorbance at 615 nm). The background was subtracted from both of the above measurements, and the absorbance of the blue dye following pumping as a percentage of the absorbance at 100% exchange was calculated. Figure 4B shows that, with some bank-to-bank and test-to-test variability, the exchange efficiency in the wells overall was near, and often greater, than 90%.

***EcAMSat* payload exerts additional stress, but can reproduce the *rpoS*-dependent UPEC resistance to Gm.** We next determined if the AB method can be used to assess Gm's effect on the two UPEC strains in the *EcAMSat* payload system, using absorbance changes at the same three wavelengths as the well-plate measurements and converting absorbance as described above to quantities of oxidized and reduced AB (Figure 5A). The environment provided by this system for the cells is closed and exposes them to its potentially stressful constituents, such as poly(methylmethacrylate), the acrylic-based pressure-sensitive adhesive, and poly(styrene); it was therefore not surprising that cells in this setup grew more slowly: some 20 hours were required for growth completion (Figure 5B), as opposed to six hours in conventional flasks (Materials and Methods). Given this relative sluggishness, we extended the starvation, Gm-treatment, and AB-viability phases of the experiments to 30, 45, and 50 hours, respectively (see Figure 5A).

The reduction of AB by wild type and mutant strains, both untreated and gentamicin-treated (52 μg/mL), is shown in Figures 6A and 6B, respectively. As in the well-plate experiments, no change in the cell-related turbidity occurred during the experiment for either strain, indicating absence of growth (Figure 6A, B: black and gray curves). There was a more marked difference in the metabolic activity of the untreated wild type and the mutant strains (Figure 6A) in the payload setup than was seen in the microplate experiments (Figure 3C). Given that the payload environment is stressful and absence of the *rpoS* gene broadly weakens UPEC,[4] this was expected and necessitated, as in the well-plate experiments, normalization of the effect of Gm on the two strains to take into account this baseline difference.

Figure 6C shows the (un-normalized) relative concentration vs. time of the oxidized form of AB for both the wild type (black/grey curves) and mutant (green curves) strains for all Gm doses: control, low (3.5 µg/mL), medium (14.6 µg/mL), and high (52 µg/mL). As with the well-plate experiment, a meaningful comparison of the relative activity of Gm-treated wild type and mutant strains required normalization for their respective untreated levels of activity. This was done as described above (Figure 6D). To enable comparison with the well-plate experiments, we chose for the results shown in Figure 6D the time point at which the Gm-treated wild type control had reduced 74% of the AB ($t = 11.5$ hour: see vertical red line, Figure 6C), analogous to the final time point of the well-plate experiment, at which 74% of the AB had also been reduced ($t = 6$ hour in Figure 3D, E, from which Figure 3F data were obtained). While this comparison reveals little difference between the effects of Gm on the two strains at the lower doses (Figure 6D), there is a significantly larger effect on the mutant relative to the wild type at the high dose of Gm (52 µg/mL): wild type, 74.5 ± 0.5% of untreated change; mutant, 64.1 ± 2.2% of untreated change; $p < 0.001$. This result is comparable to the well-plate result, albeit at a higher Gm dose. The reason why the mutant exhibits differential sensitivity only at higher drug concentration is not clear and would require further work to disentangle the interaction between the stresses of the payload system and that exerted by Gm. Nevertheless, it is clear that the system designed here is capable of answering the basic queries of interest, namely, would space MG increase Gm resistance of UPEC and would it do so in an *rpoS*-dependent manner?

**Determination of bacterial viability and reagent strength with 'aging' during the stasis period.** For our upcoming *EcAMSat* spaceflight experiment, there is some uncertainty concerning the interval of time that will elapse between the loading and integration of all payload constituents, including the bacteria in stasis, and the start of the experiment onboard the nanosatellite in a stable Earth orbit: it could exceed six weeks. Accordingly, we determined the effect of such a stasis period on bacterial viability and reagent strength; based on experience with *PharmaSat*, tests were conducted for a stasis period of ca. 10 weeks. Consistent with previous studies,[5] the Δ*rpoS* mutant retained less viability compared to the wild type: 0.3 vs. 0.7%. Gm was found to lose some 50% of its potency. These differences will be compensated for by appropriately adjusting the loading concentrations. AB and LB did not change their potency during this period.

## DISCUSSION

Concern about human health during space travel has been of central interest since the inclusion of humans in space flights. Chief among these have been issues such as the effects of microgravity on bone density, muscle strength, and cardiac function; to these, more recently have been added the potential dangers of greater susceptibility of humans to infectious disease.[28,29]

There is compelling evidence that human immune response is compromised in space flight.[28] Thus, after space flight, the oxidative burst capacity of monocytes and neutrophils of astronauts is diminished, as are the functions of their natural killer and T cells; cytokine production patterns are altered, likely accounting for the reactivation of herpesviruses seen in astronauts; stress hormones are increased; and there is a tendency to shift to the Th2 pattern (cytokine secretion resembling that of Th2 lymphocytes). Exposure to hypoxia or hyperoxia within the spacecraft or during spacewalks can further weaken the immune response.[11,30-32]

This danger is compounded by the possibility that bacteria become more virulent in microgravity. Wilson *et al*.[33] showed that, following culture on the Space Shuttle, *S*. *Typhimurium* became more virulent in mice. Furthermore, the bulk of evidence, gathered in LSMMG studies, indicates that bacteria may become more resistant in MG to disinfectant agents, such as high salt and ethanol[8] and, as we show here, including an important antibiotic.

Bacterial antibiotic resistance has been examined also in actual MG during space flights, but the results have been contradictory. Thus, while cultivation onboard Salyut 7 resulted in an increase in the minimum inhibitory concentration (MIC) of *E*. *coli* to colistin and kanamycin,[34] studies on the Space Station MIR indicated mostly decreased MIC to several antibiotics.[35] These pioneering studies indicating at least the possibility of increased bacterial drug resistance in space require further in-depth examination. It is towards this end that we have developed and tested the payload system described here. We demonstrate that our microfluidic cards and fluid delivery systems, along with the capability of AB to indicate *E*. *coli* viability, can be effectively used with space experimentation hardware and protocols. In combination with the advantages conferred by the use of nanosatellite systems, this platform provides an excellent approach for an in-depth study of bacterial drug resistance during space flight.

The dependence on $\sigma^s$ of LSMMG-conferred heightened resistance of UPEC to Gm that we show here is akin to the role of this sigma factor in this resistance seen under Earth gravity.[5]

The latter studies identified several proteins of the antioxidant defense of this bacterium that can be targeted to enhance the efficacy of this drug. Examples span reactive-oxygen-species (ROS) quencher proteins (e.g., superoxide dismutase and catalase); and those of the pentose phosphate pathway that supply the NADPH that the quencher proteins require for their activity (e.g., glucose-6-phosphate, the phosphogluconate dehydrogenases, and transaldolase A). We are at present screening small compound libraries for inhibiting these proteins that could conceivably be used in synergy with Gm to enhance its efficacy. If the space experiment corroborates the LSMMG effect of $\sigma^s$-dependence of Gm resistance, such inhibitor compounds could prove valuable in combating UTI in astronauts during space travel. Also, the behavior of the Δ*rpoS* mutant in inflight experiments will critically test whether the findings of the LSMMG studies, namely that *E. coli* perceives MG as a stress, are accurate.

Like the effect of space MG on drug resistance, other aspects of microbial biology have been reported to be affected differently by this gravity condition in different studies. In several experiments on US Space Shuttle missions, Klaus *et al*. reported a shorter lag phase and a longer exponential phase compared to ground controls,[36] ascribing this effect to the formation of a ‘pseudo-membrane’ in the form of an osmotic solute gradient interfering with nutrient flux to the cells. However, it has been reported[37,38] that spaceflight affected neither the lag nor the exponential phase in *E. coli*. Our planned spaceflight experiments promise to shed light on these questions as well.

# Legends

**Figure 1.** Schematic diagram of *EcAMSat* fluidic system (at left) connected to *EcAMSat* 48-well fluidic card (at lower right). A single fluidic well is also shown in cross section (top right). SV = 3-way solenoid valve; green arrows show direction of fluid flow; Waste H, M, L, C collect the flow-through from the High, Medium, Low, and Control banks of 12 wells each; other components are as marked.

**Figure 2.** **A)** Fully assembled *EcAMSat* biological/fluidic/optical/thermal payload system; **B)** its hermetic payload containment vessel with electrical interface board; overall size ~ 10 x 10 x 20 cm. **C)** Chronological summary of the sequence of operations and measurements for the ground experiments conducted to date; the spaceflight system will follow the same timeline.

**Figure 3.** **A**) Counts of colony-forming units for wild type (WT) and Δ*rpoS* mutant strains of *E. coli* without and with gentamicin ("Gm") treatment at 16 μg/mL (reproduced from ref. 39 for convenience of references). **B**) Color changes of Alamar Blue in 96-well plates due to metabolism of treated and untreated WT and Δ*rpoS* mutant; well rows are aligned to corresponding bars of Panel A; control row ("AB + M9") shows initial, unchanged blue color of AB in the absence of cellular metabolism. **C**) Time dependence of relative concentrations of oxidized (blue/turquoise curves) and reduced (pink/magenta curves) forms of AB along with OD (turbidity; black/grey curves) due to wild type ("WT") and mutant ("Mut") cells in absence of Gm measured with a wellplate reader. **D**) Same measurement as in Panel C but in the presence of 16 μg/mL Gm. **E**) Time dependence of concentration of blue (oxidized) AB for each strain (WT in black/grey; mutant in green/light green) without and with Gm treatment. **F**) Relative magnitude of the effect of Gm on the two strains based on the $t$ = 6-hour data from Panel E; each

bar is normalized to the amount of AB reduction measured for the respective strain in absence of Gm treatment ($n = 6$; $p < 0.0001$). Error bars in Panels C through F are ± one standard deviation.

**Figure 4.** **A**) Expected (calculated) and optically measured (using dye) equivalent doses of Gm prepared using three separate "builds" of the *EcAMSat* fluidic system (different fluidic cards, tubing sets, pumps, and valves) for dye concentrations corresponding to low, medium, and high Gm levels. **B**) Optically measured exchange efficiency of *EcAMSat* fluidic wells after ~ 400 μL of exchange fluid were pumped through each 100 μL well by the fluidic system for the four banks of wells depicted in Figure 1; all wells contained stationary-phase *E. coli* in order to include their impact on flow resistance through 0.2 μm pore-size filters at the inlet and outlet of each well ($n = 12$ per condition per test). Error bars in both panels are ± one standard deviation.

**Figure 5.** **A**) Time-dependent changes during growth, antibiotic-treatment, and Alamar-Blue-measurement phases of experiment using the *EcAMSat* optical system, fluidic card, and fluidic delivery system. Curves show absorbance of oxidized (blue/turquoise curves) and reduced (pink/magenta curves) forms of AB along with OD (turbidity; black/grey curves) due to wild type ("WT") and mutant ("Mut") cells. **B**) Semi-log plot of OD due to cells (turbidity) from the growth phase of Panel A for wild type (black) and mutant (green) strains, showing the different growth phases. Error bars in both panels are ± one standard deviation.

**Figure 6.** **A**) Time dependence of absorbance due to oxidized (blue/turquoise) and reduced (pink/magenta) forms of AB along with OD due to cells (turbidity; black/grey) for both *E. coli* strains in absence of Gm. **B**) As in Panel A, but treated with Gm at 52 μg/mL. **C**) Alamar Blue reduction curves (absorbance vs. time) for Gm = 0, 3.5, 14.6, and 52 μg/mL; diagonal arrows start at control (Gm = 0), point through low and medium doses, and terminate at highest dose. Line at $t = 11.5$ hour denotes point at which WT control has reduced 77% of

Alamar Blue, equivalent to the $t = 6$ hour data point of the conventional well-plate experiment shown in Figure 3. **D**) Amount of Alamar Blue reduced in presence of 3.5, 14.6, and 52 µg/mL Gm (“Low”, “Medium”, “High”) normalized to the amount of AB reduced for the untreated control for each strain at $t = 11.5$ hour of Panel C; $p < 0.0001$ for the high Gm dose. Error bars for Panels A, B, and D are ± one standard deviation.

## ACKNOWLEDGMENTS

This research was supported by NASA grant NNX10AM90A to A.M. at Stanford and by NASA’s Space Life and Physical Sciences Research Division, Human Exploration and Operations Mission Directorate, at NASA Ames Research Center (ARC).

## CONTRIBUTIONS

The study was originally conceived by ACM and built upon as work progressed by NASA/ARC colleagues. The *EcAMSat* payload system, based on the previously flown PharmaSat spaceflight payload,[13,14] was adapted in order to execute the experiments reported here. Changes in system architecture and design were conceived by AJR, CCB, MPP, MC, and CRF. The biology experiment was adapted for compatibility with the *EcAMSat* payload hardware by MPP, MPL, and SC, who also conducted biology labwork at ARC with the participation of MRP and TNC. The fluidics system, with integrated optical measurement capability, was modified, developed, extensively tested and calibrated by MRP, TNC, MPL, MC, SSR, CMM, DTW, MXT, TDB, and CCB. Software and mechanical engineering work on the *EcAMSat* payload was accomplished by MC, CCB, AC, TVS, and CRF. AJR, MRP, and MPP developed and implemented data analysis methods. MBH managed NASA engineering configuration and documentation and SMS is the

NASA *EcAMSat* project manager. J-HW and MK carried out experimental work at Stanford. ACM, MRP, MPP, and AJR wrote the manuscript.

# REFERENCES

1. Hengge-Aronis R. Signal transduction and regulatory mechanisms involved in control of the sigma(S) (*RpoS*) subunit of RNA polymerase. Microbiol Mol Biol Rev. 2002; **66**(3):373-395, table of contents.
2. Matin A. The molecular basis of carbon-starvation-induced general resistance in *Escherichia coli*. Molecular microbiology. 1991; **5**(1):3-10.
3. Matin A. Stress, Bacterial: General and Specific. In: Editor-in-Chief: Moselio S, editor. Encyclopedia of Microbiology (Third Edition). Oxford: Academic Press; 2009. pp. 485-500.
4. Matin AC. Stress, Bacterial: General and Specific. Reference Module in Biomedical Sciences: Elsevier; 2014.
5. Wang JH, Singh R, Benoit M, Keyhan M, Sylvester M, Hsieh M, *et al*. Sigma S-dependent antioxidant defense protects stationary-phase *Escherichia coli* against the bactericidal antibiotic gentamicin. Antimicrob Agents Chemother. 2014; **58**(10):5964-5975.
6. Lynch SV, Brodie EL, Matin A. Role and regulation of sigma S in general resistance conferred by low-shear simulated microgravity in *Escherichia coli*. J Bacteriol. 2004; **186**(24):8207-8712.
7. Lynch SV, Mukundakrishnan K, Benoit MR, Ayyaswamy PS, Matin A. *Escherichia coli* biofilms formed under low-shear modeled microgravity in a ground-based system. Appl Environ Microbiol. 2006; **72**(12):7701-7710.
8. Singh R, Matin AC. Cellular Response of *Escherichia coli* to Microgravity and Microgravity Analogue Culture. In: Nickerson AC, Pellis RN, Ott MC, editors. Effect of Spaceflight and Spaceflight Analogue Culture on Human and Microbial Cells: Novel Insights into Disease Mechanisms. New York, NY: Springer New York; 2016. pp. 259-282.
9. Bascove M, Huin-Schohn C, Gueguinou N, Tschirhart E, Frippiat JP. Spaceflight-associated changes in immunoglobulin VH gene expression in the amphibian *Pleurodeles waltl*. FASEB J. 2009; **23**(5):1607-1615.
10. Crucian BE, Stowe RP, Mehta SK, Yetman DL, Leal MJ, Quiriarte HD, *et al*. Immune status, latent viral reactivation, and stress during long-duration head-down bed rest. Aviat Space Environ Med. 2009; **80**(5 Suppl):A37-A44.
11. Mehta SK, Stowe RP, Feiveson AH, Tyring SK, Pierson DL. Reactivation and shedding of cytomegalovirus in astronauts during spaceflight. J Infect Dis. 2000; **182**(6):1761-1764.
12. Nicholson WL, Ricco AJ, Agasid E, Beasley C, Diaz-Aguado M, Ehrenfreund P, *et al*. The *O/OREOS* mission: first science data from the Space Environment Survivability of Living Organisms (SESLO) payload. Astrobiology. 2011; **11**(10):951-958.
13. Parra M, Ly D, Ricco AJ, McGinnis MR, Niesel D. The *PharmaSat* Nanosatellite platform for life science experimentation: effects of spaceflight on antifungal activity against *Saccharomyces cerevisiae*. Gravitational and Space Biology. 2009; **23**(30):30.
14. Ricco AJ, Parra M, Niesel D, Piccini M, Ly D, McGinnis M, *et al*. *PharmaSat*: drug dose response in microgravity from a free-flying integrated biofluidic/optical culture-and-analysis

satellite. Proc. SPIE 7929, Microfluidics, BioMEMS, and Medical Microsystems IX. SPIE: Bellingham, WA, 2011:79290T (9 pp).

15. Woellert K, Ehrenfreund P, Ricco AJ, Hertzfeld H. Cubesats: Cost-effective science and technology platforms for emerging and developing nations. Advances in Space Research. 2011; **47**(4):663-684.

16. Zgurskaya HI, Keyhan M, Matin A. The sigma S level in starving *Escherichia coli* cells increases solely as a result of its increased stability, despite decreased synthesis. Mol Microbiol. 1997; **24**(3):643-651.

17. Kolter R, Siegele DA, Tormo A. The stationary phase of the bacterial life cycle. Annu Rev Microbiol. 1993; **47**:855-874.

18. Sonenshein AL. CodY, a global regulator of stationary phase and virulence in Gram-positive bacteria. Curr Opin Microbiol. 2005; **8**(2):203-207.

19. Llorens JM, Tormo A, Martínez-García E. Stationary phase in gram-negative bacteria. FEMS Microbiol Rev. 2010; **34**(4):476-495.

20. Cabeen MT. Stationary phase-specific virulence factor overproduction by a lasR mutant of *Pseudomonas aeruginosa*. PLoS One. 2014; **9**(2):e88743.

21. Mouslim C, Hughes KT. The effect of cell growth phase on the regulatory cross-talk between flagellar and Spi1 virulence gene expression. PLoS Pathog. 2014; **10**(3):e1003987.

22. Dalebroux ZD, Svensson SL, Gaynor EC, Swanson MS. ppGpp conjures bacterial virulence. Microbiol Mol Biol Rev. 2010; **74**(2):171-199.

23. Roop II RM, Gee JM, Robertson GT, Richardson JM, Ng WL, Winkler ME. *Brucella* stationary-phase gene expression and virulence. Annu Rev Microbiol. 2003; **57**:57-76.

24. Mangan MW, Lucchini S, Danino V, Croinin TO, Hinton JC, Dorman CJ. The integration host factor (IHF) integrates stationary-phase and virulence gene expression in *Salmonella enterica serovar Typhimurium*. Molecular microbiology. 2006; **59**(6):1831-1847.

25. Kau AL, Hunstad DA, Hultgren SJ. Interaction of uropathogenic *Escherichia coli* with host uroepithelium. Curr Opin Microbiol. 2005; **8**(1):54-59.

26. Kau AL, Martin SM, Lyon W, Hayes E, Caparon MG, Hultgren SJ. *Enterococcus faecalis* tropism for the kidneys in the urinary tract of C57BL/6J mice. Infect Immun. 2005; **73**(4):2461-2468.

27. Matin A, Auger EA, Blum PH, Schultz JE. Genetic basis of starvation survival in nondifferentiating bacteria. Annu Rev Microbiol. 1989; **43**:293-316.

28. Yi B, Crucian B, Tauber S, Ullrich O, Choukèr A. Immune Dysfunction in Spaceflight: An Integrative View. In: Nickerson AC, Pellis RN, Ott MC, editors. Effect of Spaceflight and Spaceflight Analogue Culture on Human and Microbial Cells: Novel Insights into Disease Mechanisms. New York, NY: Springer New York; 2016. pp. 61-79.

29. Barrila J, Wilson JW, Soni A, Yang J, Mark Ott C, Nickerson CA. Using Spaceflight and Spaceflight Analogue Culture for Novel Mechanistic Insight into *Salmonella* Pathogenesis. In: Nickerson AC, Pellis RN, Ott MC, editors. Effect of Spaceflight and Spaceflight Analogue Culture on Human and Microbial Cells: Novel Insights into Disease Mechanisms. New York, NY: Springer New York; 2016. pp. 209-235.

30. Gueguinou N, Huin-Schohn C, Bascove M, Bueb JL, Tschirhart E, Legrand-Frossi C, *et al*. Could spaceflight-associated immune system weakening preclude the expansion of human presence beyond Earth's orbit? J Leukoc Biol. 2009; **86**(5):1027-1038.

31. Stowe RP, Sams CF, Pierson DL. Adrenocortical and immune responses following short- and long-duration spaceflight. Aviat Space Environ Med. 2011; **82**(6):627-634.

32. Stowe RP, Kozlova EV, Sams CF, Pierson DL, Walling DM. Latent and lytic Epstein-Barr virus gene expression in the peripheral blood of astronauts. J Med Virol. 2011; **83**(6):1071-1077.

33. Wilson JW, Ott CM, Honer zu Bentrup K, Ramamurthy R, Quick L, Porwollik S, *et al*. Space flight alters bacterial gene expression and virulence and reveals a role for global regulator Hfq. Proc Natl Acad Sci U S A. 2007; **104**(41):16299-16304.

34. Tixador R, Richoilley G, Gasset G, Planel H, Moatti N, Lapchine L, *et al*. Preliminary results of Cytos 2 experiment. Acta Astronaut. 1985; **12**(2):131-134.

35. Juergensmeyer MA, Juergensmeyer EA, Guikema JA. Long-term exposure to spaceflight conditions affects bacterial response to antibiotics. Microgravity Sci Technol. 1999; **12**(1):41-47.

36. Klaus D, Simske S, Todd P, Stodieck L. Investigation of space flight effects on *Escherichia coli* and a proposed model of underlying physical mechanisms. Microbiology. 1997; **143** (Pt 2):449-455.

37. Kacena MA, Merrell GA, Manfredi B, Smith EE, Klaus DM, Todd P. Bacterial growth in space flight: logistic growth curve parameters for *Escherichia coli* and *Bacillus subtilis*. Appl Microbiol Biotechnol. 1999; **51**(2):229-234.

38. Vukanti R, Model MA, Leff LG. Effect of modeled reduced gravity conditions on bacterial morphology and physiology. BMC Microbiol. 2012; **12**:4.

39. Zhang Y, Lai C, Duan J, Guan N, Ullah K, Deng Y. Simulated microgravity affects semicarbazide-sensitive amine oxidase expression in recombinant *Escherichia coli* by HPLC-ESI-QQQ analysis. Appl Microbiol Biotechnol. 2012; **94**(3):809-816.

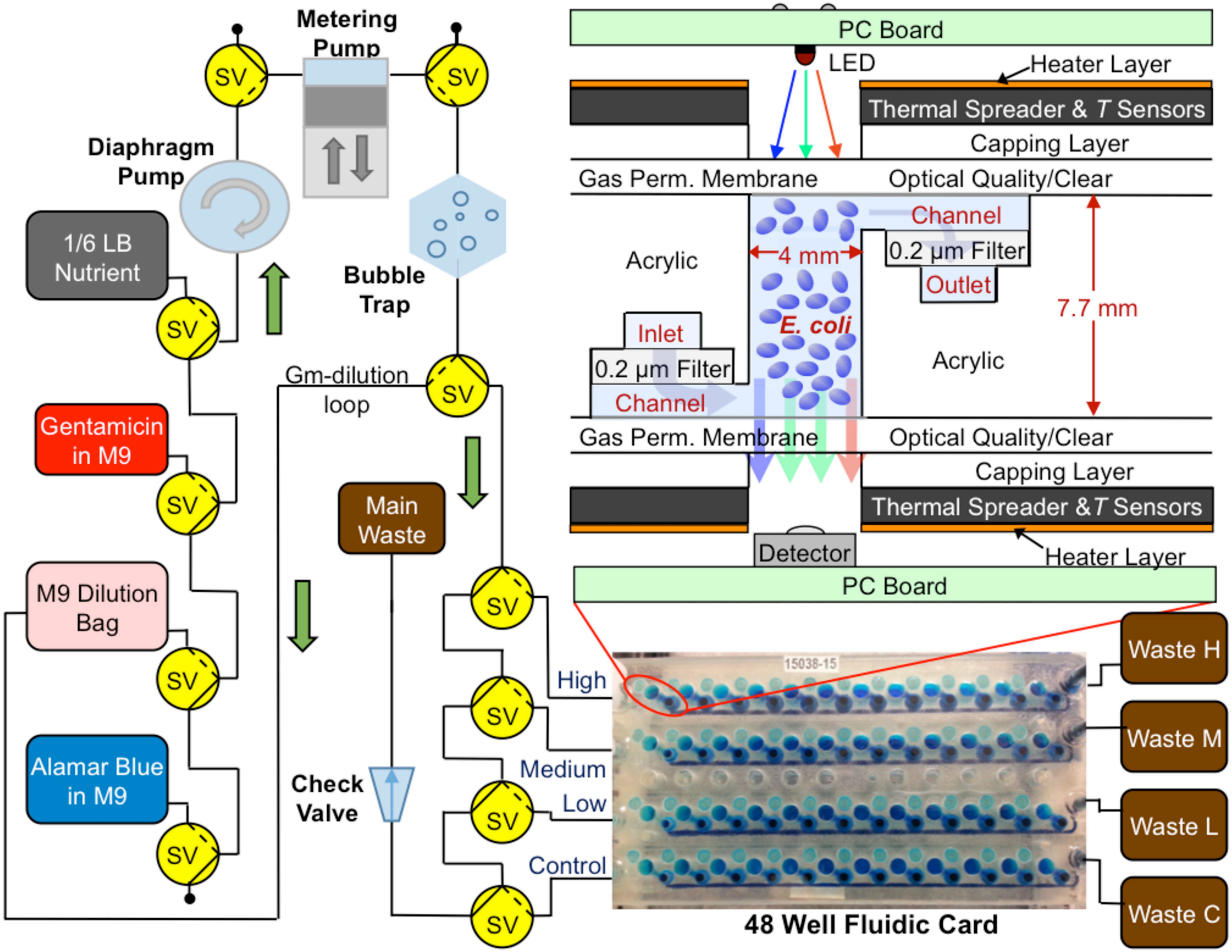
Metering Pump
SV
SV
Diaphragm Pump
1/6 LB Nutrient
SV
Bubble Trap
Gm-dilution loop
SV
Gentamicin in M9
SV
Main Waste
M9 Dilution Bag
SV
SV
High
SV
Medium
Low
Alamar Blue in M9
SV
SV
Check Valve
Control
SV
PC Board
LED
Heater Layer
Thermal Spreader & T Sensors
Capping Layer
Gas Perm. Membrane
Optical Quality/Clear
Channel
0.2 μm Filter
Outlet
Acrylic
4 mm
7.7 mm
E. coli
Inlet
0.2 μm Filter
Channel
Acrylic
Gas Perm. Membrane
Optical Quality/Clear
Capping Layer
Thermal Spreader & T Sensors
Detector
Heater Layer
PC Board
15038-15
Waste H
Waste M
Waste L
Waste C
48 Well Fluidic Card

Figure 1

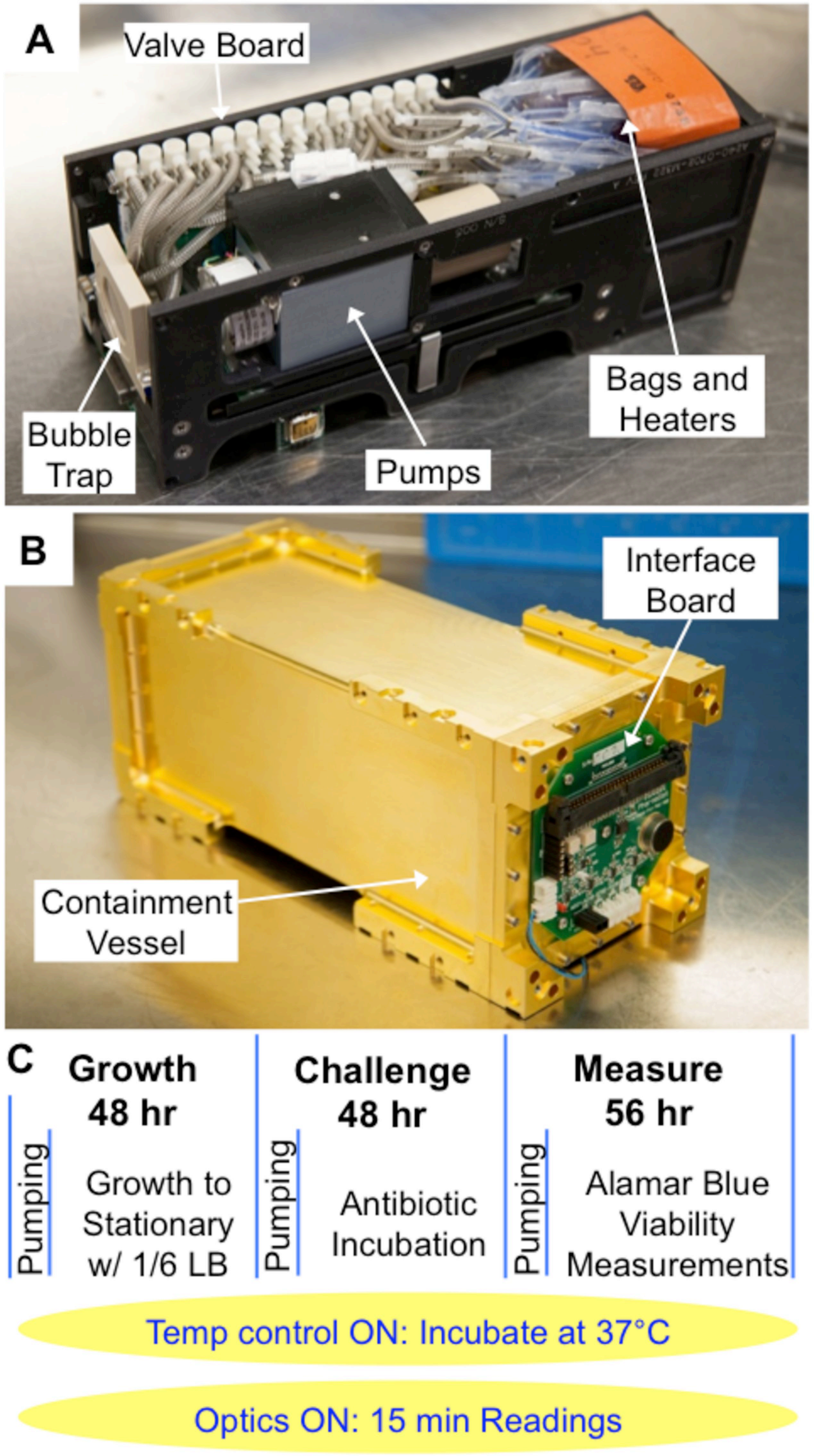
A
Valve Board
Bubble Trap
Pumps
Bags and Heaters
B
Interface Board
Containment Vessel
C
Growth 48 hr
Pumping
Growth to Stationary w/ 1/6 LB
Challenge 48 hr
Pumping
Antibiotic Incubation
Measure 56 hr
Pumping
Alamar Blue Viability Measurements
Temp control ON: Incubate at 37°C
Optics ON: 15 min Readings

Figure 2

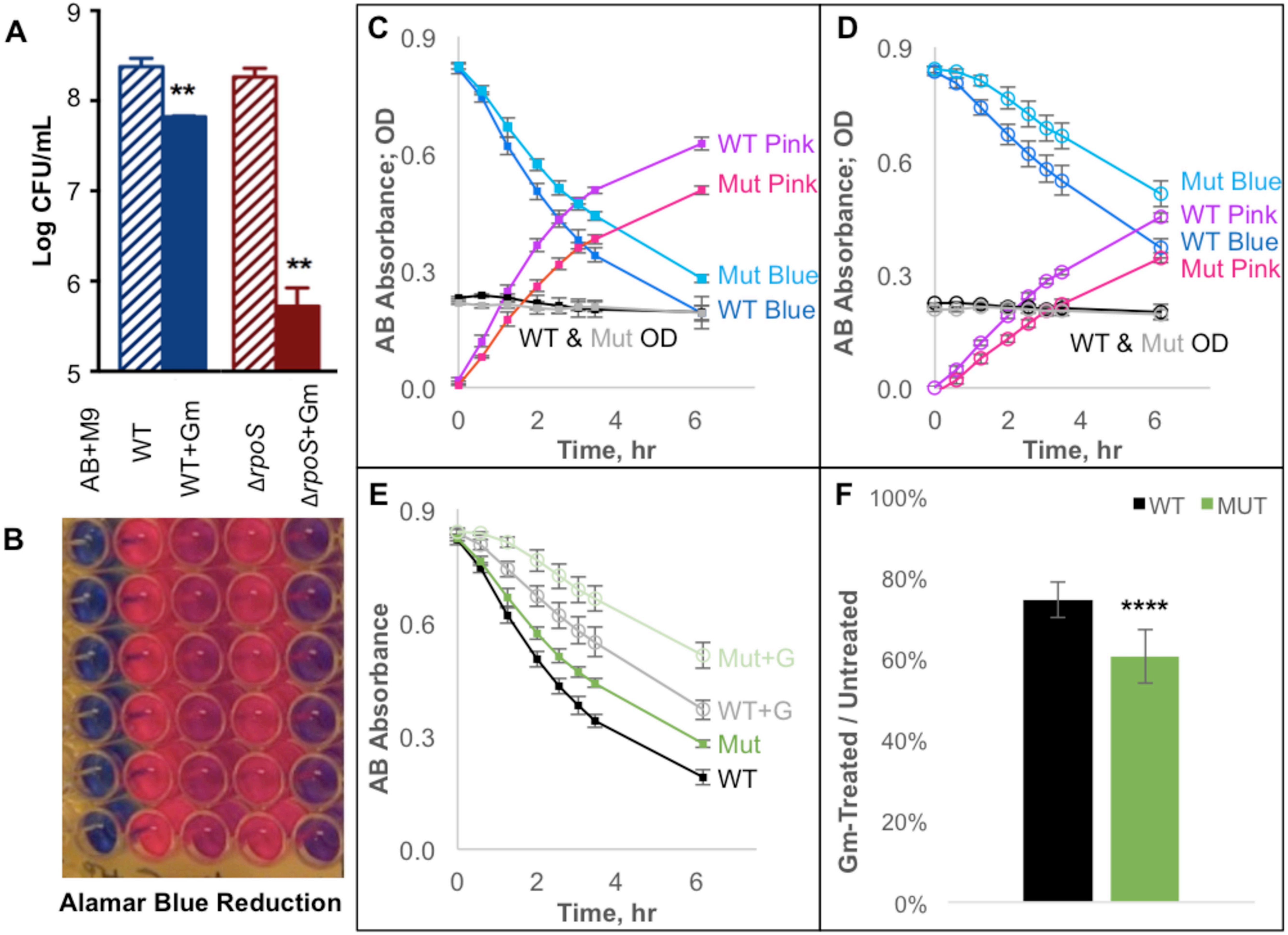
A
Log CFU/mL
9
8
7
6
5
**
**
AB+M9
WT
WT+Gm
ΔrpoS
ΔrpoS+Gm
B
Alamar Blue Reduction
C
AB Absorbance; OD
0.9
0.6
0.3
0.0
0
2
4
6
Time, hr
WT Pink
Mut Pink
Mut Blue
WT Blue
WT & Mut OD
D
AB Absorbance; OD
0.9
0.6
0.3
0.0
0
2
4
6
Time, hr
Mut Blue
WT Pink
WT Blue
Mut Pink
WT & Mut OD
E
AB Absorbance
0.9
0.6
0.3
0.0
0
2
4
6
Time, hr
Mut+G
WT+G
Mut
WT
F
Gm-Treated / Untreated
100%
80%
60%
40%
20%
0%
■WT ■MUT
****

Figure 3

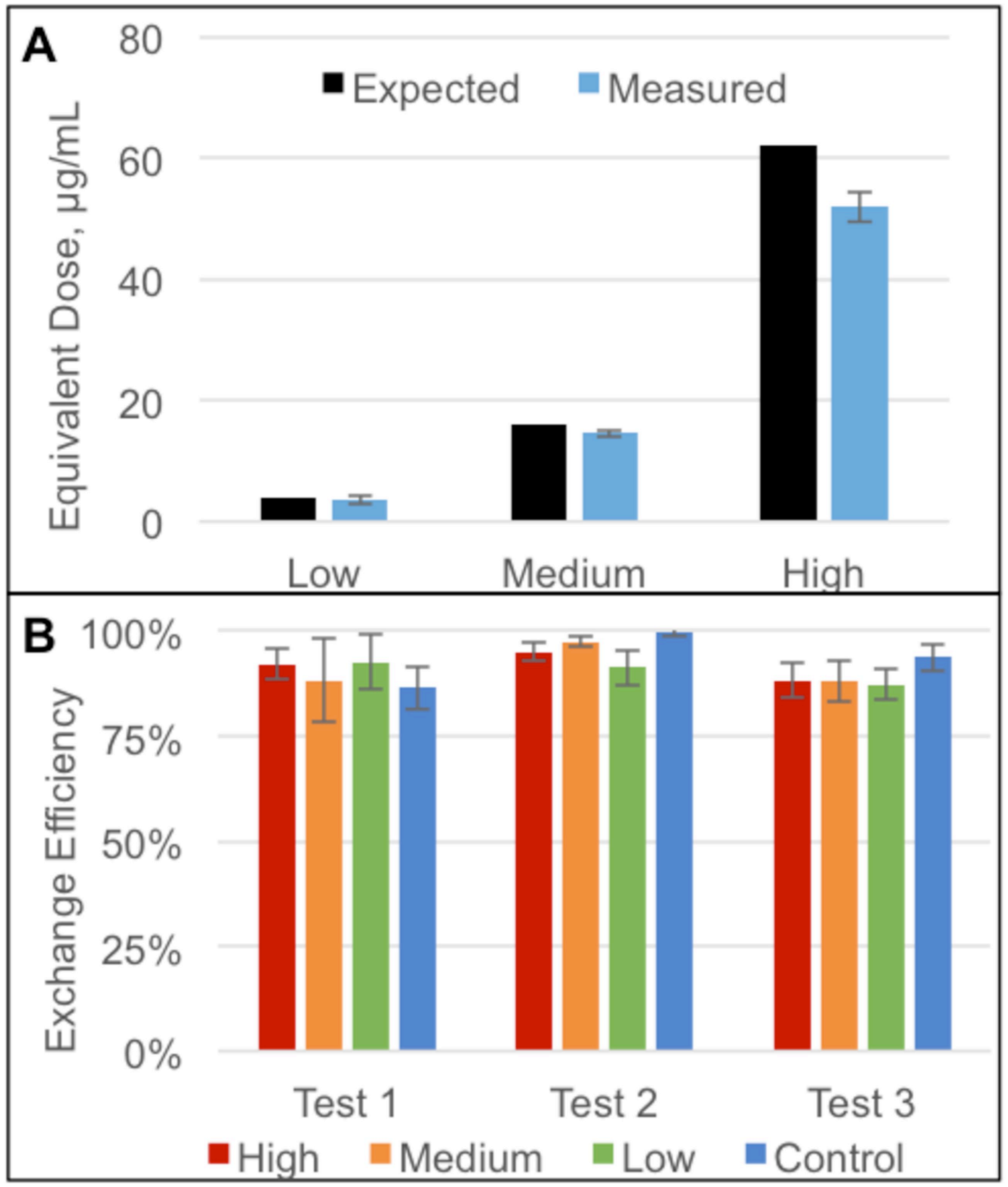
A
B
Equivalent Dose, μg/mL
0
20
40
60
80
Expected
Measured
Low
Medium
High
Exchange Efficiency
0%
25%
50%
75%
100%
Test 1
Test 2
Test 3
High
Medium
Low
Control

Figure 4

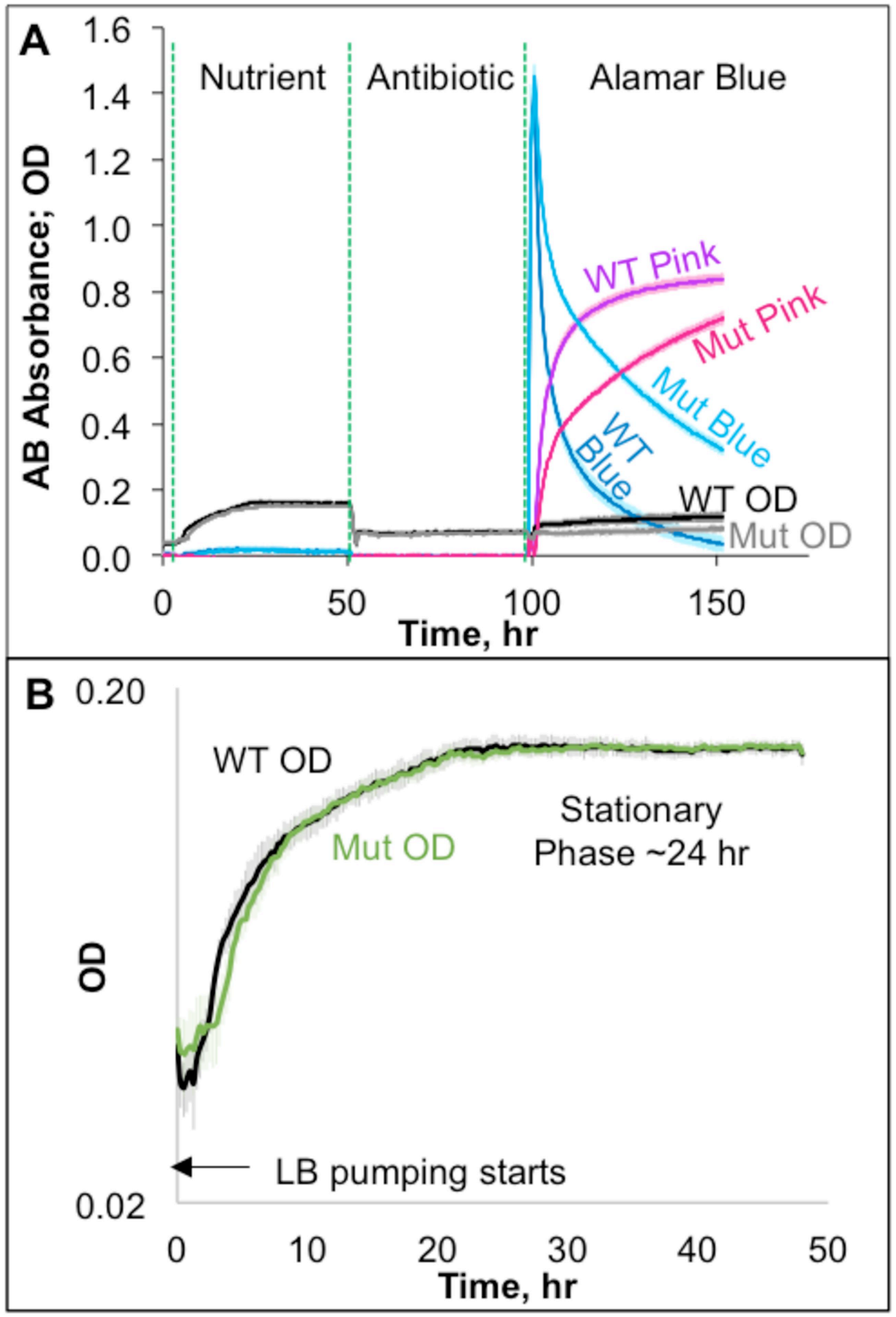
A
1.6
1.4
1.2
1.0
0.8
0.6
0.4
0.2
0.0
AB Absorbance; OD
Nutrient
Antibiotic
Alamar Blue
WT Pink
Mut Pink
Mut Blue
WT Blue
WT OD
Mut OD
0
50
100
150
Time, hr
B
0.20
0.02
OD
WT OD
Mut OD
Stationary Phase ~24 hr
LB pumping starts
0
10
20
30
40
50
Time, hr

Figure 5

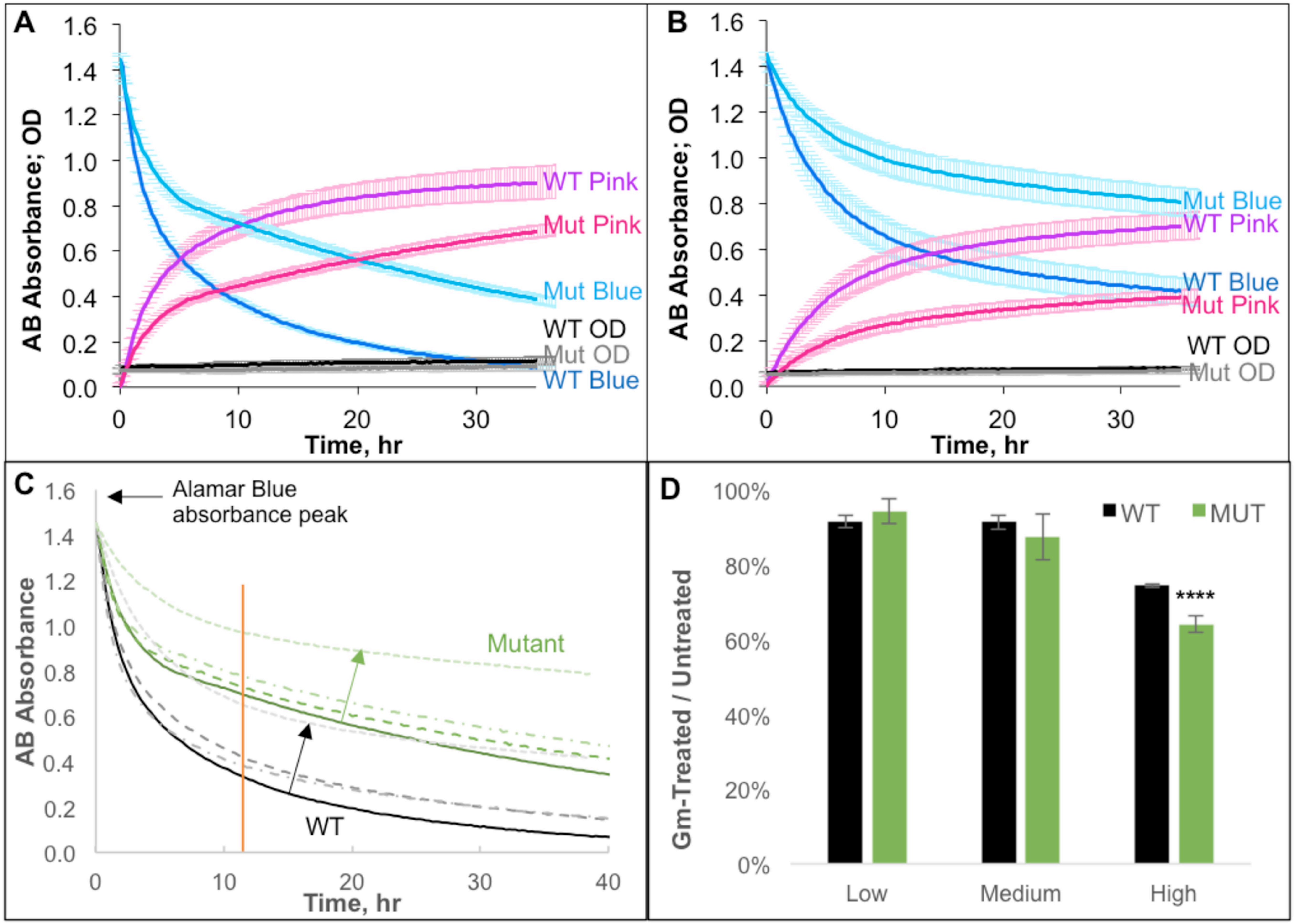
A
1.6
1.4
1.2
1.0
0.8
0.6
0.4
0.2
0.0
AB Absorbance; OD
WT Pink
Mut Pink
Mut Blue
WT OD
Mut OD
WT Blue
0
10
20
30
Time, hr
B
1.6
1.4
1.2
1.0
0.8
0.6
0.4
0.2
0.0
AB Absorbance; OD
Mut Blue
WT Pink
WT Blue
Mut Pink
WT OD
Mut OD
0
10
20
30
Time, hr
C
Alamar Blue
absorbance peak
1.6
1.4
1.2
1.0
0.8
0.6
0.4
0.2
0.0
AB Absorbance
Mutant
WT
0
10
20
30
40
Time, hr
D
100%
80%
60%
40%
20%
0%
Gm-Treated / Untreated
WT
MUT
****
Low
Medium
High

Figure 6